Journal of Southeast University (English Edition) Vol. 40, No. 3, pp. 238 - 244 Sept. 2024 ISSN 1003—7985

Analysis on flutter performance of flexible photovoltaic support based on full-order method

Zhou Rui Wang Hao Xu Zidong

(Key Laboratory of Concrete and Prestressed Concrete Structures of Ministry of Education, Southeast University, Nanjing 211189, China)

Abstract: Taking a three-cable flexible photovoltaic (PV) support structure as the research subject, a finite element model was established. Utilizing a full-order flutter analysis method, the flutter critical wind speed and flutter frequency of the flexible PV support structure at a tilt angle of 0° were calculated. The results showed good agreement with wind tunnel test data. Further analysis examined the pretension effects in the load-bearing and stabilizing cables on the natural frequency and flutter critical wind speed of the flexible PV support structure. The research findings indicate increasing the pretension in the load-bearing cables significantly raises the natural frequencies of the first four modes. Specifically, as the pretension in the load-bearing cables increases from 22 to 102 kN, the flutter critical wind speed rises from 17.1 to 21.6 m/s. By contrast, the pretension in the stabilizing cable has a smaller effect on the natural frequency and flutter critical wind speed of the flexible PV support structure. When the pretension in the stabilizing cable increased from 22 to 102 kN, the flutter critical wind speed increased from 17.1 to 17.7 m/s. For wind-resistant design of flexible PV support structures, it is recommended to prioritize increasing the pretension in the load-bearing cables to enhance the structural flutter performance.

Key words: flexible photovoltaic support; flutter critical wind speed; full-order method; finite element model

DOI: 10.3969/j.issn.1003-7985.2024.03.003

Large-span flexible photovoltaic (PV) support structures typically employ a prestressed cable tensioning system to create a wide layout of PV modules, demonstrating excellent adaptability to different terrains. Compared to traditional support structures, these large-span systems are more flexible, with increased support and component heights, making them more susceptible to wind forces. Studying the wind resistance performance of flexible structures is essential for ensuring structural safety[1-2]. The PV modules, resembling thin plates in cross-section, have a low first-order torsional bending frequency ratio, which reduces the critical wind speed for flutter-induced vibrations[3]. There have been significant instances of wind-induced vibrations and damage in flexible PV supports, highlighting the urgent need for a systematic study of their flutter performance.

While there is extensive research on the wind resistance of fixed PV support systems[4-5], studies on flexible PV systems are scarce. Du et al.[6] conducted wind tunnel experiments to investigate the wind pressure characteristics of PV panels, developing a finite element model to study the effects of wind direction and speed on the wind-induced vibration response of flexible PV support structures. Ma et al.[7] conducted wind tunnel experiments to assess how wind direction angle, module tilt angle, module spacing ratio, and installation position affect PV panel wind loads. He et al.[8-9] proposed a novel flexible PV support system, investigating its load-bearing capacity under self-weight, wind loads, snow pads, and their combined effects. Liu et al.[10] proposed three methods to reduce vibrations in flexible PV supports and validated their effectiveness through a series of wind tunnel experiments. More recently, researchers have focused on the flutter performance of flexible PV supports. Li et al.[11] conducted wind tunnel experiments to investigate this, exploring the effectiveness of two aerodynamic measures in enhancing flutter stability. Chen et al.[12] studied the aerodynamic stability of a single-row flexible PV support under different tilt angles, wind angles, and uniform turbulent wind fields. They further investigated the interference effects on PV supports at a 10° tilt angle by changing the wind angle, the number of PV supports, and their connections. These investigations underscore a considerable lack of research on the flutter performance of flexible PV supports. The impact of structural parameters on the critical wind speed for flutter remains unclear, emphasizing the need for further investigation into their flutter performance.

This paper focuses on a flexible PV support from existing literature, using it as the engineering background to develop a finite element model based on ANSYS software. The full-order method is employed to solve the

Received 2024-03-12, **Revised** 2024-05-20.

Biographies: Zhou Rui (1999—), male, Ph.D. candidate; Wang Hao (corresponding author), male, doctor, professor, wanghao1980@seu.edu.cn.

Foundation items: The National Natural Science Foundation of China (No. 52338011, 52208481), China Postdoctoral Science Foundation (No. 2023M730581).

Citation: Zhou Rui, Wang Hao, Xu Zidong. Analysis on flutter performance of flexible photovoltaic support based on full-order method [J]. Journal of Southeast University (English Edition), 2024, 40(3): 238 - 244. DOI: 10.3969/j.issn.1003-7985.2024.03.003.

structural flutter frequency and flutter critical wind speed, and these results are compared with wind tunnel test data. The study calculates the critical flutter wind speeds of the flexible PV support structure under 9 different conditions. It also analyzes the impact of pretension in both the load-bearing and stabilizing cables on the flutter performance. The research findings provide valuable insight into optimizing the wind-resistant design of flexible PV supports.

1 Finite Element Model

1.1 Model parametric

A flexible PV support structure with a span of 35 m, as shown in Fig. 1, employs three steel cables to support the PV modules. Each span contains a total of 28 PV modules. These modules are directly supported by two load-bearing cables, which are connected through a stabilizing cable through triangular brackets made of hollow round steel pipes. Four triangular supports are placed at the 6th, 12th, 16th, and 22nd PV modules, respectively. The dimensions of each PV module are 2.256 m × 1.133 m × 0.035 m (length × width × thickness), with a tilt angle of 15° and a net spacing of 50 mm between adjacent PV modules. The mass of each PV module is 32.3 kg. The pretension forces in the load-bearing cables and stabilizing cables are 21.8 and 42.1 kN, respectively.

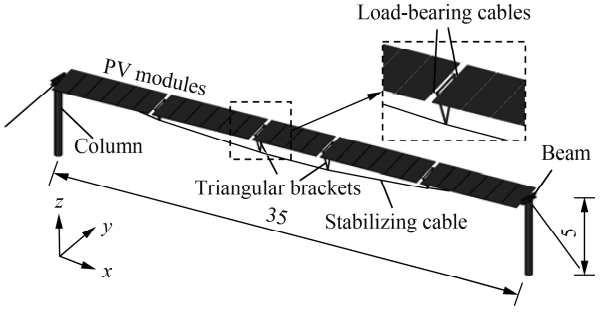

Fig. 1 Flexible PV support structures (unit: m)

1.2 Modal analysis

A finite element model of the flexible PV support structure was created using ANSYS software. The columns and I-beams were simulated using the "Beam188" element, while the cables and PV modules were modeled with the "Link10" and "Shell63" elements, respectively. The triangular brackets were simulated using the "Link180" element.

To verify the accuracy of the finite element model, modal analysis was conducted using the Block Lanczos method. The first 10 orders of modes of the flexible PV support were obtained, as shown in Table 1. Fig. 2 illustrates the mode shapes of the first four orders. The first two-order modes of the flexible support structure are the first-order symmetrical vertical bending and the first-order symmetrical torsion, with frequencies of 1.09 Hz and 1.37 Hz, respectively. These results are almost consistent with those calculated results by Li et al.[11], showing errors of 1.9% and 3.5% for the first two natural frequencies. This validates the effectiveness of the finite element model and provides a basis for flutter analysis. Additionally, the third mode is anti-symmetric vertical bending, with a natural frequency very close to that of the second mode. The fourth mode is a composite of lateral bending and torsion.

Table 1 First ten-order modes of the flexible PV support

Order	Frequency/Hz	Mode shape	Order	Frequency/Hz	Mode shape
1	1.09	S-V-1	6	2.55	AS-V-2
2	1.37	S-T-1	7	3.08	AS-T-1
3	1.38	AS-V-1	8	3.09	AS-VT-1
4	1.77	S-LT-1	9	3.49	AS-V-2
5	1.99	S-V-2	10	3.59	AS-LT-1

Notes: S represents symmetric; AS represents antisymmetric; V represents vertical; L represents lateral; T represents torsional; LT represents lateral coupled torsional; VT represents vertical coupled torsional; the number indicates the order of appearance of the mode.

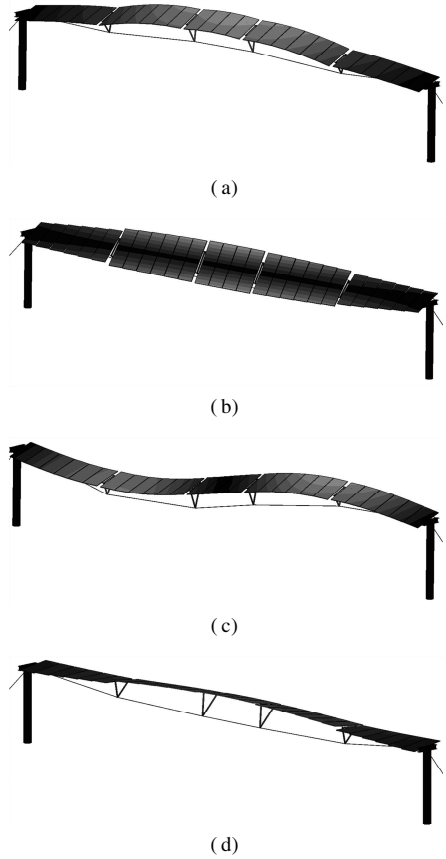

Fig. 2 First four-order mode shapes of the flexible PV support. (a) S-V-1; (b) S-T-1; (c) AS-V-1; (d) S-LT-1

2 Full-Order Flutter Analysis Method

2.1 Scanlan self-excited force model

The phenomenon of flutter in bridges has been extensively studied[13-14]. Flexible PV support structures are

similar to large-span cable-supported bridge structures. The motion equations of a flexible PV support structure in uniform flow can be described as follows:

$$\boldsymbol{M}\ddot{\boldsymbol{X}} + \boldsymbol{C}\dot{\boldsymbol{X}} + \boldsymbol{K}\boldsymbol{X} = \boldsymbol{F}_{\mathrm{se}} \tag{1}$$

where $\boldsymbol{M}$, $\boldsymbol{C}$, and $\boldsymbol{K}$ represent the mass, damping, and stiffness matrices of the structure, respectively; $\boldsymbol{X}$, $\dot{\boldsymbol{X}}$, and $\ddot{\boldsymbol{X}}$ represent the nodal displacement, velocity, and acceleration vectors, respectively; $\boldsymbol{F}_{\mathrm{se}}$ represents the self-exciting force.

According to the Scanlan self-excited force model[15], the lift (L_{se}), drag (D_{se}), and torque (M_{se}) distributed along the structural unit length can be expressed in terms of flutter derivatives related to the amplitude:

$$L_{\mathrm{se}} = \frac{1}{2}\rho U^2(2B)\left(KH_1^*\frac{\dot{h}}{U} + KH_2^*\frac{B\dot{\alpha}}{U} + K^2H_3^*\alpha + K^2H_4^*\frac{h}{B} + KH_5^*\frac{\dot{p}}{U} + K^2H_6^*\frac{p}{B}\right) \tag{2}$$

$$D_{\mathrm{se}} = \frac{1}{2}\rho U^2(2B)\left(KP_1^*\frac{\dot{p}}{U} + KP_2^*\frac{B\dot{\alpha}}{U} + K^2P_3^*\alpha + K^2P_4^*\frac{p}{B} + KP_5^*\frac{\dot{h}}{U} + K^2P_6^*\frac{h}{B}\right) \tag{3}$$

$$M_{\mathrm{se}} = \frac{1}{2}\rho U^2(2B^2)\left(KA_1^*\frac{\dot{h}}{U} + KA_2^*\frac{B\dot{\alpha}}{U} + K^2A_3^*\alpha + K^2A_4^*\frac{h}{B} + KA_5^*\frac{\dot{p}}{U} + K^2A_6^*\frac{p}{B}\right) \tag{4}$$

where U is the mean wind velocity; ρ is the air density; B is the cross-sectional width; $K = B\omega/U$ is the reduced frequency; ω is the structural circular frequency; h, p, and α represent the vertical, lateral, and torsional displacements, respectively; $\dot{h}$, $\dot{p}$, and $\dot{\alpha}$ are the vertical, lateral, and torsional velocity, respectively; H_i^*, P_i^*, and A_i^* ($i = 1, 2, \ldots, 6$) indicate amplitude-dependent flutter derivatives.

The aerodynamic forces described by Eqs. (2)-(4) represent the distributed loads along the structural unit length. In finite element analysis, these distributed loads are converted into equivalently concentrated loads acting on the nodes of the elements[16]. Therefore, the equivalent aerodynamic force acting on element e can be expressed in terms of node displacements and node velocities as follows:

$$\boldsymbol{F}_{\mathrm{se}}^e = \boldsymbol{K}_{\mathrm{se}}^e\boldsymbol{X}^e + \boldsymbol{C}_{\mathrm{se}}^e\dot{\boldsymbol{X}}^e \tag{5}$$

where $\boldsymbol{F}_{\mathrm{se}}^e$ is the self-exciting force of element e; $\boldsymbol{X}^e$ and $\dot{\boldsymbol{X}}^e$ are the node displacement and node velocity vectors of element e, respectively; $\boldsymbol{K}_{\mathrm{se}}^e$ and $\boldsymbol{C}_{\mathrm{se}}^e$ are the aerodynamic stiffness matrix and aerodynamic damping matrix of element e, respectively. When using the lumped aerodynamic moment matrix, the expressions for $\boldsymbol{K}_{\mathrm{se}}^e$ and $\boldsymbol{C}_{\mathrm{se}}^e$ are as follows:

$$\boldsymbol{C}_{\mathrm{se}}^e = \begin{bmatrix} \boldsymbol{C}_{\mathrm{se1}}^e & 0 \\ 0 & \boldsymbol{C}_{\mathrm{se2}}^e \end{bmatrix},\ \boldsymbol{K}_{\mathrm{se}}^e = \begin{bmatrix} \boldsymbol{K}_{\mathrm{se1}}^e & 0 \\ 0 & \boldsymbol{K}_{\mathrm{se2}}^e \end{bmatrix} \tag{6}$$

$$\boldsymbol{C}_{\mathrm{se1}}^e = a\begin{bmatrix} 0 & 0 & 0 & 0 & 0 & 0 \\ 0 & P_1^* & P_5^* & BP_2^* & 0 & 0 \\ 0 & H_5^* & H_1^* & BH_2^* & 0 & 0 \\ 0 & BA_5^* & BA_1^* & B^2A_2^* & 0 & 0 \\ 0 & 0 & 0 & 0 & 0 & 0 \\ 0 & 0 & 0 & 0 & 0 & 0 \end{bmatrix}$$

$$\boldsymbol{K}_{\mathrm{se1}}^e = b\begin{bmatrix} 0 & 0 & 0 & 0 & 0 & 0 \\ 0 & P_4^* & P_6^* & BP_3^* & 0 & 0 \\ 0 & H_6^* & H_4^* & BH_3^* & 0 & 0 \\ 0 & BA_6^* & BA_4^* & B^2A_3^* & 0 & 0 \\ 0 & 0 & 0 & 0 & 0 & 0 \\ 0 & 0 & 0 & 0 & 0 & 0 \end{bmatrix}$$

where $a = \rho UBKL_e/2$ and $b = \rho U^2K^2L_e/2$; L_e represents the length of element e.

2.2 Flutter analysis based on ANSYS

From Eq. (6), when all flutter derivatives of the PV panel are known, the coefficients in the aerodynamic stiffness and aerodynamic damping matrices can be determined. The aerodynamic forces on the two nodes of element e can then be fully calculated based on the displacements and velocities at these nodes. Owing to the difficulty in directly obtaining the flutter derivatives of the PV panel, this study focuses solely on the flutter performance of the flexible PV support structure at a 0° tilt angle for ease of computation. The flutter derivatives for the PV panel at a 0° tilt angle can be approximated using those of an ideal plate[17]. Fig. 3 provides the flutter derivatives for the ideal plate at different reduced wind speeds $U/(fB)$. Here, f means the structure frequency.

Inspired by wind-resistant studies on bridges[18-19], a full-order flutter analysis method is used to calculate the critical wind speed at which flutter occurs in the flexible PV support structure. In ANSYS, the Matrix27 element is used to simulate the aerodynamic self-excited forces, as it allows for defining kinematic responses through stiffness, damping, or mass coefficients. Therefore, the aerodynamic self-excited force on the PV panel can be simulated using the Matrix27 element. Each PV panel is connected to two pairs of Matrix27 elements: one pair simulates aerodynamic damping, while the other pair simulates aerodynamic stiffness. The full-order method involves solving the complex eigenvalues (λ_i) of the structure at different wind speeds to track changes in the real and imaginary parts. The specific steps are outlined below:

1) Establishing the original finite element model to obtain the natural frequencies ω_i^0 ($i = 1, 2, \ldots, m$) for the first m modes.

2) Adding Matrix27 elements to the original finite element model and storing the flutter derivatives.

3) Setting the initial search wind speed U_0 and the wind speed increment ΔU.

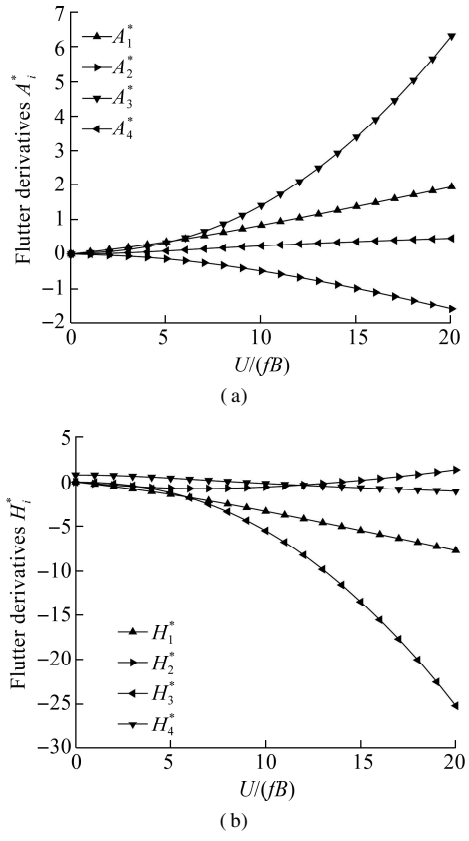

Fig. 3 Flutter derivatives of an ideal flat plate. (a) Torsional flutter derivatives A_i^*; (b) Vertical flutter derivatives H_i^*

4) Selecting the i-th modal branch to track, assuming that the initial frequency of the tracked mode (ω_i) is equal to the structural natural frequency (ω_i^0).

5) Calculating the reduced wind speed for the current iteration, determining the aerodynamic stiffness and the aerodynamic damping matrix, and then performing a complex eigenvalue analysis.

6) Measuring the error between the imaginary part of the i-th complex eigenvalue $\mathrm{Im}(\lambda_i)$ and the trial frequency ω_i. If the error is less than 0.001, set $\omega_i = \mathrm{Im}(\lambda_i)$, then repeat Steps 5) and 6). If not, proceed to Step 7).

7) Repeat Steps 4 through 6 for all m computed natural modes to obtain all m pairs of complex eigenvalues at the present wind velocity U. If the real parts of all complex eigenvalues $\mathrm{Re}(\lambda_i)$ ($i = 1, 2, \ldots, m$) are negative, set $U = U_0 + \Delta U$ and repeat Steps 4) to 6). Otherwise, terminate the iteration.

This iterative process is facilitated through parametric programming with ANSYS parametric design language. The full-order flutter analysis process is illustrated in Fig. 4.

3 Flutter Calculation of Flexible PV Support

Before flutter occurs, the flexible PV support structure exhibits considerable rigidity, resulting in relatively small vibration amplitudes. Therefore, this paper ignores the geometric nonlinearity of the flexible PV support structure

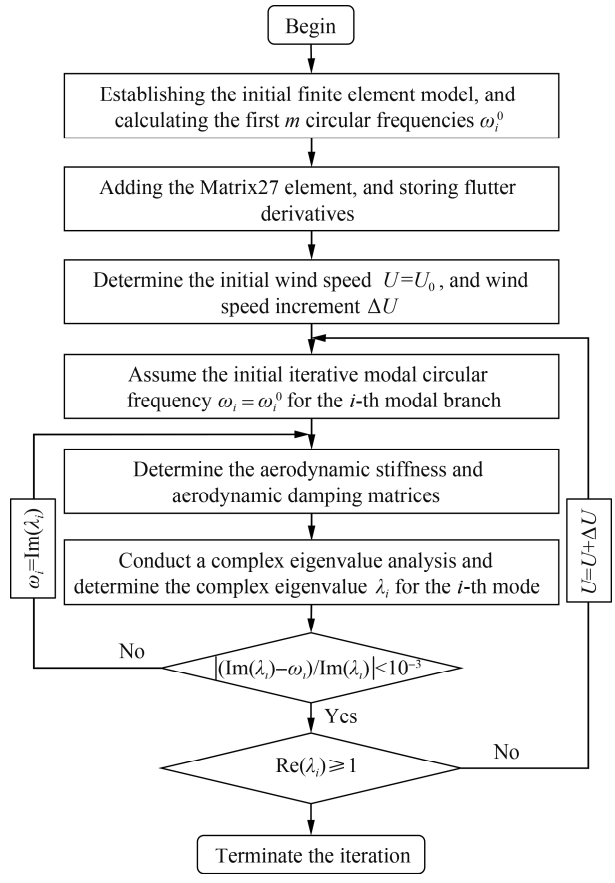

Fig. 4 Full-order flutter analysis flowchart

and conducts a linear flutter analysis to evaluate the critical flutter wind speed. The critical flutter wind speed is determined by considering the first four modes of the structure in the full-modal calculation, with a damping ratio of 0.02. It should be noted that changing the tilt angle of the PV modules does not alter their mode shapes. The criterion for determining the critical flutter wind speed is that the real part of any complex eigenvalue becomes positive. Fig. 5 illustrates the variations in the real and imaginary parts of the first four complex modes with wind speed. As shown in Fig. 5, as wind speed increases, the real parts of the 1st and 3rd-order modes decrease, while the real part of the 4th-order mode remains almost constant. The real part of the 2nd-order mode decreases initially, then increases until it changes from negative to positive. At a wind speed of 17.1 m/s, the real part is exactly 0, indicating that the flexible PV support is in a critical flutter state. This suggests that the critical wind speed for the 0° tilt angle flexible PV support is 17.1 m/s, with a corresponding flutter frequency (imaginary part) of 1.169 Hz. When flutter occurs, the dominant mode is a coupled vertical and torsional vibration.

The comparison between the finite element model's calculations and the wind tunnel test results is presented in Table 2. The wind tunnel test results indicate a flutter critical wind speed of 17.8 m/s and a flutter frequency of

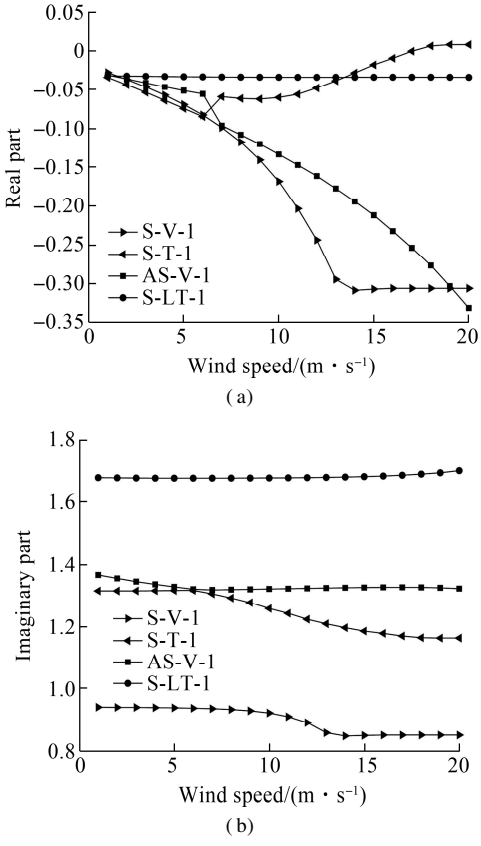

Fig. 5 Variation in the complex eigenvalues with wind speed. (a) Real part; (b) Imaginary part

1.224 Hz for the flexible PV support at a 0° tilt angle. Compared to the wind tunnel test results, the errors in the flutter critical wind speed and flutter frequency calculated by the finite element model are within 5%. This indicates that the full-order method employed in this study accurately calculates the flutter critical wind speed of the flexible PV support structure.

Table 2 Comparison between the finite element model's calculations and wind tunnel test results

Flutter index	Wind tunnel test[11]	Finite element model	Error/%
Flutter critical wind speed/(m · s^{-1})	17.8	17.1	3.9
Flutter frequency/Hz	1.224	1.169	4.5

4 Parametric Analysis

For cable-supported PV structures, the pretension of the cables directly influences structural stiffness. To investigate how pretension affects the flutter performance, the pretension of the load-bearing cables and stabilizing cable is incrementally altered by 20 kN gradients based on the existing design scheme. Notably, when adjusting the pretension of the load-bearing cables, the pretension of the stabilizing cable remains unchanged, and vice versa.

Since structural flutter is a vibration dominated by one or several mode shapes, evaluating the dynamic characteristics of flexible PV supports with different pretension levels is important for analyzing their flutter performance. Modal analysis reveals that pretension does not affect the first four-order mode shapes of the structure. The effect of pretension on the natural frequencies of flexible PV support is shown in Fig. 6. As shown in Fig. 6(a), increasing the pretension in the load-bearing cables raises the natural frequencies of the first four-order modes. Furthermore, the rate at which the natural frequencies increase accelerates with higher mode orders. When the pretension in the load-bearing cables increases from 22 to 102 kN, the natural frequencies of the first four-order modes of the flexible PV support structure increase by 18.2%, 30.3%, 35.8%, and 43.5%, respectively. Fig. 6(b) shows no consistent trend in the variation in the natural frequencies of the first four modes with changes in the pretension of the stabilizing cable. With increased pretension, the natural frequencies of the first and third modes gradually increase, while the natural frequency of the fourth mode decreases. However, the second mode frequency initially increases and then decreases. When the pretension in the stabilizing cable increases from 22 to 102 kN, the first and third mode orders increase by 3.1% and 4.3%, respectively, while the fourth-order mode frequency decreases by 12.6%. In summary, compared to the load-bearing cables, the stabilizing cable has a relatively minor impact on the dynamic characteristics of the flexible PV support.

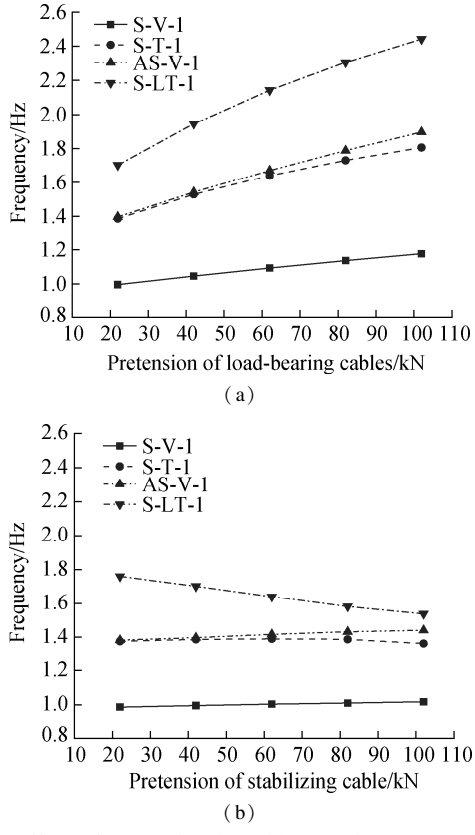

Fig. 6 Effect of pretension in cables on the structural natural frequency. (a) Load-bearing cables; (b) Stabilizing cable

The influence of pretension on the flutter critical wind speed and flutter frequency of the flexiblePV support is illustrated in Fig. 7. It can be observed that as pretension in the load-bearing cables increases, both the flutter critical wind speed and flutter frequency exhibit approximately linear growth. Specifically, when the pretension in the load-bearing cables increases from 22 to 102 kN, the flutter critical wind speed increases from 17.1 to 21.6 m/s, and the flutter frequency increases from 1.169 to 1.484 Hz. However, changes in the pretension of the stabilizing cable have minimal impact. When the pretension in the stabilizing cable increases from 22 to 82 kN, there is little to no change in either the flutter critical wind speed or flutter frequency. Even at a pretension of 102 kN, the flutter critical wind speed increases to 17.7 m/s, a marginal rise of 0.6 m/s. From these observations, it is evident that increasing the pretension in the load-bearing cables significantly enhances the flutter critical wind speed of the flexible PV support structure. However, changes in the pretension of the stabilizing cable do not appreciably affect the flutter critical wind speed. This difference can be attributed to the relationship between critical flutter wind speed and structural stiffness: higher structural stiffness leads to a higher critical flutter wind speed. As shown in Fig. 6, increasing the pretension in the load-bearing cables significantly raises the structural natural frequencies of the structure compared to the stabilizing cable. This indicates that enhancing the pretension of the load-bearing cables has a more pronounced effect on increasing the structural stiffness.

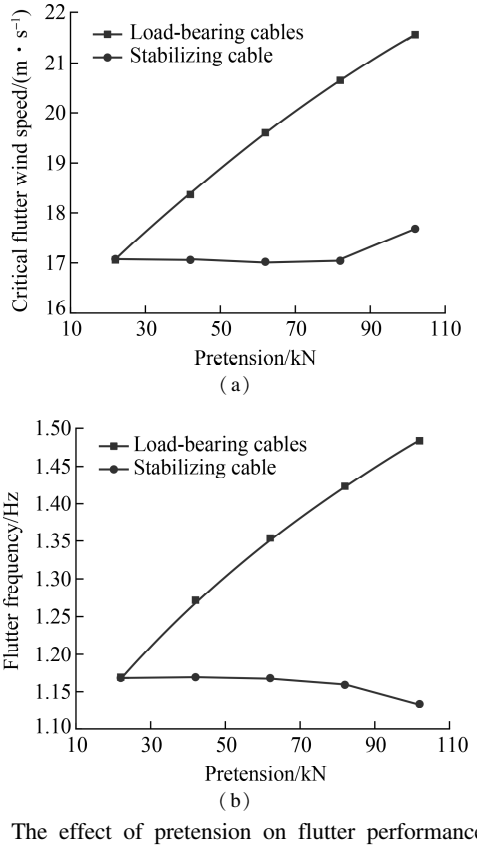

Fig. 7 The effect of pretension on flutter performance. (a) Critical flutter wind speed; (b) Flutter frequency

5 Conclusions

1) The full-order method based on the finite element model is suitable for calculating the flutter critical wind speed of flexible PV support structures. The computed results align well with wind tunnel test results, with errors in the flutter critical wind speed and flutter frequency calculations within 5% of experimental values.

2) The pretension in the load-bearing cables significantly affects the natural frequencies of flexible PV support structures, while the pretension in the stabilizing cable has a minor effect. Increasing the cable pretension does not alter the first four orders of mode shapes.

3) Increasing the pretension in the load-bearing cables from 22 to 102 kN resulted in a 4.5 m/s increase in the flutter critical wind speed. However, increasing the pretension in the stabilizing cable had a negligible effect on the flutter critical wind speed. Therefore, in structural design, priority should be given to increasing the pretension in the load-bearing cables to enhance the flutter performance of flexible PV support structures.

References

[1] Tao T Y, Gao W J, Jiang Z X, et al. Analysis on wind-induced vibration and its influential factors of long suspenders in the wake of bridge tower[J]. *Journal of Southeast University (Natural Science Edition)*, 2023, **53**(6): 1065 - 1071. DOI: 10.3969/j.issn.1001-0505.2023.06.013. (in Chinese)

[2] Lin Y X, Xu Z D, Wang H, et al. Analysis of wind vibration response of suspended derrick under downburst [J]. *Journal of Southeast University (Natural Science Edition)*, 2023, **39**(4): 333 - 339. DOI: 10.3969/j.issn.1003-7985.2023.04.002. (in Chinese)

[3] Chen Z Q. *Bridge wind engineering*[M]. Beijing: China Communications Press, 2005: 86 - 98.

[4] Alrawashdeh H, Stathopoulos T. Wind loads on solar panels mounted on flat roofs: Effect of geometric scale [J]. *Journal of Wind Engineering and Industrial Aerodynamics*, 2020, **206**: 104339. DOI: 10.1016/j.jweia.2020.104339.

[5] Reina G P, de Stefano G. Computational evaluation of wind loads on sun-tracking ground-mounted photovoltaic panel arrays[J]. *Journal of Wind Engineering and Industrial Aerodynamics*, 2017, **170**: 283 - 293. DOI: 10.1016/j.jweia.2017.09.002.

[6] Du H, Xu H, Zhang Y, et al. Wind pressure characteristics and wind vibration response of long-span flexible photovoltaic support structure[J]. *Journal of Harbin Institute of Technology*, 2022, **54**(10): 67 - 74. DOI: 10.11918/202112064. (in Chinese)

[7] Ma W Y, Chai X B, Ma C C. Experimental study on wind load influencing factors of flexible support photovoltaic modules[J]. *Acta Energiae Solaris Sinica*, 2021, **42**(11): 10 - 18. DOI: 10.19912/j.0254-0096.tynxb.

2019-1184. (in Chinese)
[8] He X H, Ding H, Jing H Q, et al. Wind-induced vibration and its suppression of photovoltaic modules supported by suspension cables[J]. *Journal of Wind Engineering and Industrial Aerodynamics*, 2020, **206**: 104275. DOI: 10.1016/j.jweia.2020.104275.
[9] He X H, Ding H, Jing H Q, et al. Mechanical characteristics of a new type of cable-supported photovoltaic module system[J]. *Solar Energy*, 2021, **226**: 408 - 420. DOI: 10.1016/j.solener.2021.08.065.
[10] Liu J Q, Li S Y, Luo J, et al. Experimental study on critical wind velocity of a 33-meter-span flexible photovoltaic support structure and its mitigation[J]. *Journal of Wind Engineering and Industrial Aerodynamics*, 2023, **236**: 105355. DOI: 10.1016/j.jweia.2023.105355.
[11] Li S Y, Ma J, Liu J Q, et al. Experimental study for flutter performance of flexible photovoltaic system by segmental model test[J]. *China Civil Engineering Journal*, 2024, **57**(2): 25 - 34. DOI: 10.15951/j.tmgcxb.22111107. (in Chinese)
[12] Chen Q, Niu H W, Li H X, et al. Aerodynamic stability and interference effect on a flexible photovoltaic based on wind tunnel test with aeroelastic model[J]. *Journal of Building Structure*, 2023, **44**(11): 153 - 161. DOI: 10.14006/j.jzjgxb.2022.0891. (in Chinese)
[13] Wen X H, Wang H, Zhang H, et al. Application of overset grid technology in identification of aerodynamic parameters of flat steel box girder of suspension bridge [J]. *Journal of Southeast University* (*Natural Science Edition*), 2022, **52**(5): 841 - 847. DOI: 10.3969/j.issn.1001-0505.2022.05.003. (in Chinese)
[14] Lang T Y, Wang H, Jia H Z, et al. Vortex-induced vibration performance and wind pressure distribution of main girder of long-span suspension bridge affected by temporary facilities[J]. *Journal of Southeast University* (*Natural Science Edition*), 2022, **52**(5): 833 - 840. DOI: 10.3969/j.issn.1001-0505.2022.05.002. (in Chinese)
[15] Scanlan R H, Tomko J J. Airfoil and bridge deck flutter derivatives[J]. *Journal of the Engineering Mechanics Division*, 1971, **97**(6): 1717 - 1737. DOI: 10.1061/jmcea3.0001526.
[16] Li K, Han Y, Song J, et al. Three-dimensional nonlinear flutter analysis of long-span bridges by multimode and full-mode approaches[J]. *Journal of Wind Engineering and Industrial Aerodynamics*, 2023, **242**: 105554. DOI: 10.1016/j.jweia.2023.105554.
[17] Simiu E, Yeo D. *Wind effects on structures*[M]. New York, USA: Wiley, 2019: 20 - 35.
[18] Hua X G, Chen Z Q. Full-order and multimode flutter analysis using ANSYS[J]. *Finite Elements in Analysis and Design*, 2008, **44**(9/10): 537 - 551. DOI: 10.1016/j.finel.2008.01.011.
[19] Ge Y J, Tanaka H. Aerodynamic flutter analysis of cable-supported bridges by multi-mode and full-mode approaches[J]. *Journal of Wind Engineering and Industrial Aerodynamics*, 2000, **86**(2/3): 123 - 153. DOI: 10.1016/s0167-6105(00)00007-6.

基于全阶法的柔性光伏支架颤振性能分析

周 锐 王 浩 徐梓栋

(东南大学混凝土及预应力混凝土结构教育部重点实验室, 南京 211189)

摘要:以某三索柔性光伏支架作为研究对象,建立有限元模型. 采用全阶颤振分析方法,计算了0°倾角柔性光伏支架的颤振临界风速和颤振频率,计算结果与风洞试验数据吻合良好. 进一步分析研究了承重索和稳定索预拉力对柔性光伏支架自振频率和颤振临界风速的影响. 研究结果表明:增加承重索预拉力可显著提高结构前4阶自振频率;当承重索预拉力从22 kN增加到102 kN时,颤振临界风速从17.1 m/s增加至21.6 m/s;与承重索相比,稳定索预拉力对柔性光伏支架的自振频率和颤振临界风速影响较小;当稳定索预拉力从22 kN增加到102 kN时,颤振临界风速从17.1 m/s增加至17.7 m/s. 对于柔性光伏支架的抗风设计,建议优先增加承重索预拉力以提高结构颤振性能.

关键词:柔性光伏支架;颤振临界风速;全阶法;有限元模型
中图分类号:TU399